West Chester University
Digital Commons @ West Chester University

Chemistry

College of the Sciences & Mathematics

Hierarchical Porous Silicon and Porous Silicon Nanowires Produced with Regenerative Electroless Etching (ReEtching) and Metal Assisted Catalytic Etching (MACE)

Kurt W. Kolasinski
West Chester University of Pennsylvania, kkolasinski@wcupa.edu

Bret A. Unger
West Chester University of Pennsylvania

Haibo Yu
University of Connecticut - Storrs

Alexis T. Ernst
University of Connecticut - Storrs

Mark Aindow
University of Connecticut - Storrs

See next page for additional authors

Follow this and additional works at: https://digitalcommons.wcupa.edu/chem_facpub

Part of the Materials Chemistry Commons

Recommended Citation

Authors

Kurt W. Kolasinski, Bret A. Unger, Haibo Yu, Alexis T. Ernst, Mark Aindow, Ermei Mäkilä, and Jarno Salonen

Hierarchical Porous Silicon and Porous Silicon Nanowires Produced with Regenerative Electroless Etching (ReEtching) and Metal Assisted Catalytic Etching (MACE)

Kurt W. Kolasinski,*[a] Bret A. Unger,[a] Haibo Yu,[b‡] Alexis T. Ernst,[b] Mark Aindow,[b] Ermei Mäkilä,[c] and Jarno Salonen[c]

[a] Department of Chemistry, West Chester University, West Chester, PA 19383-2115 USA
[b] Department of Materials Science & Engineering, Institute of Materials Science, University of Connecticut, Storrs, CT 06269-3136 USA
[c] Department of Physics, University of Turku, FI-20014 Turku, Finland

ReEtching produces nanostructured silicon when a catalytic agent, e.g. dissolved V_2O_5, is used to facilitate etching between Si and H_2O_2. H_2O_2 regenerates dissolved V in a 5+ oxidation state, which initiates etching by injecting holes into the Si valence band. Independent control over the extent of reaction (controlled by the amount of H_2O_2 added) and the rate of reaction (controlled by the rate at which H_2O_2 is pumped into the etchant solution) allows us to porosify Si substrates of arbitrary size, shape and doping, including wafers, single-crystal powders, polycrystalline powders, metallurgical grade powder, Si nanowires, Si pillars and Si powders that have been textured with metal-assisted catalytic etching (MACE). Similarly, improved control over the nucleation and etching in MACE is achieved by pumped delivery of reagents. Nanowires are not produced directly by MACE of powders, rather they form when a porosified layers is cleaved by capillary forces or sonication.

*E-mail: kkolasinski@wcupa.edu
‡Current address: Advanced Characterization Dept., Honeywell UOP, Des Plaines, IL 60017

Introduction

Porous Si (por-Si) and silicon nanowires (SiNW) have appeared in technologies such as bioelectronics (1), catalysis (2), nanoelectronics (3) nanomechanics (4), energetic materials (5), and micromachining (6). A great deal of interest in por-Si has been in the areas of biomaterials (7), drug delivery (8) and sensors (9) because por-Si is a biocompatible and biodegradable material (10), the biological behavior of which can be controlled by porosity and surface chemistry (11). Silicon has the greatest specific capacity among elements that alloy with lithium; thus, it is of interest in advanced battery designs (12) and its introduction into commercial batteries has begun (13). In publications (14-18) and patents (19-21), the etching of Si powders has been constrained by low efficiency and an inability to etch completely through the particle. Conventionally, stain etching is treated like a simple chemical reaction: mix together Si and the amount of oxidant required by stoichiometry to react with the quantity of Si to be etched. Stir.

Separate the porous powder from the spent etchant. Characterize the disappointing product.

Here we develop a new concept in electroless etching (22) which we call *regenerative electroless etching* (ReEtching), that is potentially applicable to any semiconductor. As shown in Fig. 1, we use a catalytic amount of V_2O_5 dissolved in HF(aq), which produces VO_2^+. This is the primary oxidant that injects holes h^+ into the Si valence band, a necessary condition for nanostructuring (23,24). VO_2^+ is an optimal oxidant for the initiation of Si electroless etching (25,26). The technique regenerates a V(V) species by using H_2O_2 (\$0.5 kg^{-1}) – an oxidant that is known *not* to produce porous Si in the absence of a metal particle catalyst (27) – in place of the vast majority of V_2O_5 (\$50 kg^{-1}), which simultaneously enhances economic viability and process control (reducing heating and eliminating precipitation of impurities).
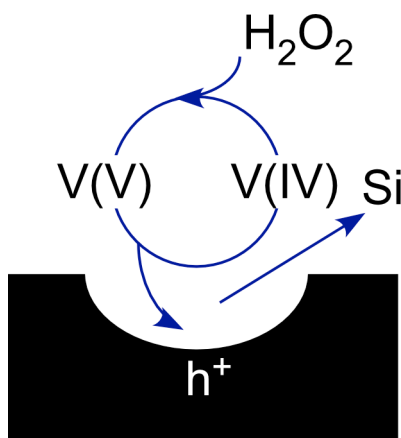

Figure 1. Schematic representation of ReEtching cycle. V(V) injects a hole h^+ to initiate the etching of a Si atom and produce reduced V(IV). H_2O_2 regenerates V(V) by oxidizing V(IV).

Results and Discussion

During etching a V(V) species is converted quantitatively to V(IV) (28). We observed (22) that H_2O_2 regenerates an oxovanadium(V) ion from the V(IV) species. We use the regeneration of V(V) by H_2O_2 as the basis of a new concept in etching. A catalytic amount of V_2O_5 is added to HF (0.05–0.5 g compared to the 6.5 g required by stoichiometry to etch 1 g of Si). After initiation of etching of Si dispersed in HF(aq) with a mixture of V_2O_5 + HF, we add H_2O_2 via a syringe pump. H_2O_2 regenerates the oxidant that initiates electroless etching. The H_2O_2 injection rate controls the rate of etching. The amount of Si etched is controlled by the amount of H_2O_2 added. Slow continuous addition of H_2O_2 reduces the thermal load on the system and produces a steady-state etch rate that facilitates thick film formation. Scaling to large batches is possible because the thermal load is greatly reduced and because a suitably low concentration of oxidant is maintained by slow addition of H_2O_2 rather than large volumes. The temperature of the reaction mixture is controlled by placing the reaction vessel, i.e. Teflon or plastic beaker, in an ice/water or thermostatted bath. The use of acetic acid as a surfactant during ReEtching greatly enhances the product yield, reduces foaming and improves homogeneity.

Hierarchical Si nanostructures containing pores within pores are produced by etching porous Si powder made by (1) pulverization of an anodized wafer, (2)

porosification of Si powder by MACE, or (3) harvesting Si nanowires from MACE-etched metallurgical-grade Si powder particles by sonication. For short, we call the material produced by ReEtching anodized porous silicon (RaPSi). Mesoporous Si or SiNW that were initially nonluminescent can be ReEtched to produce brilliantly photoluminescent powder with extremely high specific surface area. In one experiment, mesoporous powder with an initial pore size ~17 nm produced by anodization was used as starting material. ReEtching introduced ~4 nm nanopores into the walls of the mesopores. We measured specific surface areas over 400 m^2 g^{-1} from metallurgical grade powder and as high as 888 m^2 g^{-1} when ReEtching anodized porous powder. This material was ball milled to form porous nanoparticles with very high yield. Nanoparticles with a width of ~150 nm are attractive for use in intravenous drug delivery. ReEtching allowed us to create porous layers > 20 µm thick. Depending on the etching and drying conditions, such layers can result in the formation of amorphous silicon pillars that are > 20 µm in height.

ReEtching of metallurgical grade powder represents an inexpensive method of producing porous silicon powders with tortuous ~3–4 nm pores that is scalable to large quantities for use in applications such as lithium ion batteries (LIB), drug delivery and imaging enhancement. MACE of metallurgical-grade Si, as shown in Fig. 2(a), or electronics-grade, image not shown, leads to porosification of the powder particles through the formation of etch track pores. Capillary forces that arise either during etching because of bubble formation or during drying occasionally cleave the walls of the etch track pores to produce a very small number of SiNW. However, if the powder is dispersed in ethanol and subjected to ultrasonic agitation, the porous layer is rapidly removed from the porous film. The pore walls cleave at their narrowest points to produce SiNW with remarkably straight walls. The nanowires harvested from metallurgical-grade powder, Fig. 2(b), exhibit mesoporosity whereas the nanowires rendered from electronics-grade powder, Fig. 2(c), are solid core. This is consistent with the results first reported by Hochbaum et al. (29) and later confirmed by Li et al. (30) that mesoporosity is observed in etch track pore walls when MACE is performed on heavily doped wafers.
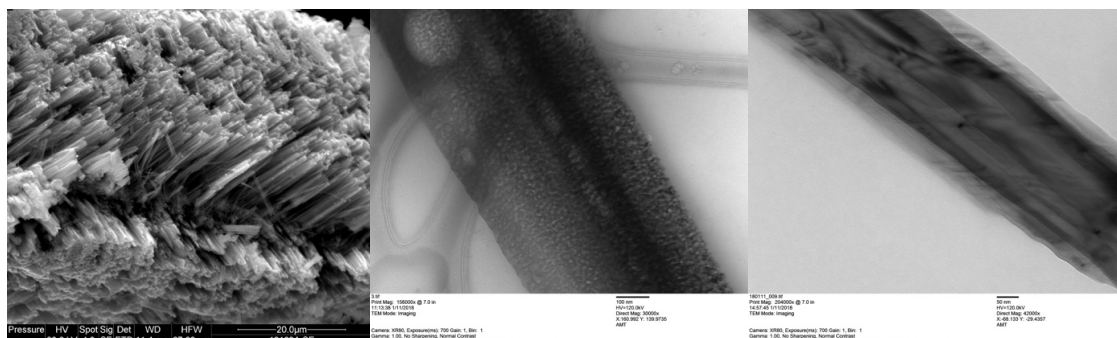
(a)   (b)   (c)

Figure 2. (a) Secondary electron scanning electron microscopy (SEM) image of metallurgical grade Si powder porosified by MACE. Cleaving the porous layer by sonicating in ethanol creates SiNW. (b) Transmission electron microscopy (TEM) image of 575 nm diameter SiNW with 6–15 nm pores from metallurgical grade Si powder. (c) TEM image of solid 350 nm diameter SiNW from electronics grade Si powder.

Photoluminescence (PL) bands from blue to red have been observed. PL in the red to near IR is extremely long lived, exhibiting multi-exponential decay with lifetime

components in excess of 100 μs. Such long-lived PL from Si nanoparticles is promising for bioimaging applications in which image acquisition is delayed after the initial photoexcitation.

Calculations of electrostatic and van der Waals forces acting between the metal nanoparticle that catalyzes MACE and the Si substrate reveal that a strong attractive force pins the catalytic nanoparticle to the Si surface throughout the etch process.

Electron microscopy reveals a strong preference for the metal nanoparticles responsible for MACE to etch along $\langle 001 \rangle$ directions. Preferential etching along the $\langle 001 \rangle$ directions has been noted previously and ascribed to a so-called backbond model (31-40), though this model has not been developed quantitatively in the literature.

We have developed a quantitative model to describe the crystallographic dependence of MACE. This model allows us to estimate the temperature dependence of the MACE etch rate, formation energy of a pore and, by extension, the preferred structure of etch-track pores/SiNW produced by MACE. The model is derived from the following ideas (1) the mean strength of a Si–Si bond E exhibits no crystallographic dependence and is equal to half the cohesive energy of Si E_c, (2) surface crystallography determines the co-ordination of Si atoms as well as the areal density of Si–Si bonds that must be broken during etching, and (3) the energy per unit area required to form an etch track pore (etch energy $\gamma_{hkl}^{\text{etch}}$) contains contributions from etching at the base of the metal nanoparticle as well as pore side-wall formation.

The details of this model will be reported elsewhere. Briefly, the expression (assuming etching in only one direction and sidewalls of only one crystallographic orientation with sidewalls perpendicular to a planar etch front) is

$$E_{\text{pore}} = \gamma_{hkl}^{\text{etch}} A_{\text{cat}} + \gamma_{hkl}'^{\text{etch}} A_{\text{sw}} \qquad [1]$$

where A_{cat} is the area beneath the catalyst, A_{sw} is the sidewall area, and $\gamma_{hkl}^{\text{etch}}$ is the energy cost per unit area of etching a plane of Si(hkl).

From the model we can conclude that the etch energy is not directly anti-correlated with the surface energy. Instead, the relationship is more complex and depends not only on the surface crystallography, which determines the number of Si–Si bonds broken per unit cell as well as the unit cell size, but also on the metal catalyst particle size. The sidewall term rapidly looses significance above ~15 nm. Interestingly this size corresponds to the size range over which the inverse (but related) vapor-liquid-solid (VLS) growth process was observed by Wu et al. (41) to undergo a change in the preferred orientation of SiNW growth. Presumably, this change in VLS growth direction is related to a similar dependence of growth direction on the balance between sidewall formation energy and growth-front formation energy.

It should be realized that metal-catalyzed etching is a kinetically controlled phenomenon. It does not produce etch track pores with the lowest possible surface energy. Instead it creates structures that are created by the lowest activation energy pathway. Therefore, the primary reason for etch-track pore formation along the $\langle 001 \rangle$ directions for isolated > 15 nm metal particles is that this is the lowest activation energy pathway. However, there is strong evidence for correlated motion between catalyst particles.

Acknowledgments

References

1.   W. Zhou, X. Dai, and C. M. Lieber, Rep Prog Phys **80**, 016701 (2017).
2.   K. Rykaczewski, O. J. Hildreth, C. P. Wong, A. G. Fedorov, and J. H. J. Scott, Nano Lett. **11**, 2369 (2011).
3.   V. Schmidt, J. V. Wittemann, and U. Gösele, Chem. Rev. **110**, 361 (2010).
4.   S. W. Schmitt, F. Schechtel, D. Amkreutz, M. Bashouti, S. K. Srivastava, B. Hoffmann, C. Dieker, E. Spiecker, B. Rech, and S. H. Christiansen, Nano Lett. **12**, 4050 (2012).
5.   C. R. Becker, S. Apperson, C. J. Morris, S. Gangopadhyay, L. J. Currano, W. A. Churaman, and C. R. Stoldt, Nano Lett. **11**, 803 (2011).
6.   J. Teva, Z. J. Davis, and O. Hansen, J. Micromech. Microeng. **20**, 015034 (2010).
7.   J. R. Henstock, L. T. Canham, and S. I. Anderson, Acta Biomaterialia **11**, 17 (2015).
8.   J. Salonen, A. M. Kaukonen, J. Hirvonen, and V. P. Lehto, J. Pharm. Sci. **97**, 632 (2008).
9.   H. Han, Z. P. Huang, and W. Lee, Nano Today **9**, 271 (2014).
10.   J. H. Park, L. Gu, G. von Maltzahn, E. Ruoslahti, S. N. Bhatia, and M. J. Sailor, Nature Mater. **8**, 331 (2009).
11.   M. Wang, P. S. Hartman, A. Loni, L. T. Canham, N. Bodiford, and J. L. Coffer, Langmuir **31**, 6179 (2015).
12.   L. Mai, X. Tian, X. Xu, L. Chang, and L. Xu, Chem. Rev. **114**, 11828 (2014).
13.   G. E. Blomgren, J. Electrochem. Soc. **164**, A5019 (2017).
14.   S. Limaye, S. Subramanian, B. Goller, J. Diener, and D. Kovalev, Phys. Status Solidi A **204**, 1297 (2007).
15.   E. G. Chadwick, N. V. V. Mogili, C. O'Dwyer, J. D. Moore, J. S. Fletcher, F. Laffir, G. Armstrong, and D. A. Tanner, Rsc Adv **3**, 19393 (2013).
16.   E. G. Chadwick, S. Beloshapkin, and D. A. Tanner, J. Mater. Sci. **47**, 2396 (2012).
17.   M. Wang, P. S. Hartman, A. Loni, L. T. Canham, and J. L. Coffer, Silicon **8**, 525 (2016).
18.   A. Loni, D. Barwick, L. Batchelor, J. Tunbridge, Y. Han, Z. Y. Li, and L. T. Canham, Electrochem. Solid State Lett. **14**, K25 (2011).
19.   Y. Li and I. Pavlovsky, Patent No. US 2004/0166319 A1 (2004).
20.   D. Farrell, S. Limaye, and S. Shanthi, Patent No. US 7560085 B2 (2007).

21.   L. T. Canham and A. Loni, Patent No. US 9540246 B2 (2017).

22.   K. W. Kolasinski, N. J. Gimbar, H. Yu, M. Aindow, E. Mäkilä, and J. Salonen, Angew. Chem., Int. Ed. Engl. **55**, 624 (2017).

23.   K. W. Kolasinski, Curr. Opin. Solid State Mater. Sci. **9**, 73 (2005).

24.   K. W. Kolasinski, Phys. Chem. Chem. Phys. **5**, 1270 (2003).

25.   K. W. Kolasinski, J. W. Gogola, and W. B. Barclay, J. Phys. Chem. C **116**, 21472 (2012).

26.   K. W. Kolasinski and J. W. Gogola, ECS Trans. **33(16)**, 23 (2011).

27.   C. Gondek, M. Lippold, I. Röver, K. Bohmhammel, and E. Kroke, J. Phys. Chem. C **118**, 2044 (2014).

28.   K. W. Kolasinski and W. B. Barclay, Angew. Chem., Int. Ed. Engl. **52**, 6731 (2013).

29.   A. I. Hochbaum, D. Gargas, Y. J. Hwang, and P. Yang, Nano Lett. **9**, 3550 (2009).

30.   X. Li, C. Yan, J. Wang, A. Graff, S. L. Schweizer, A. Sprafke, O. G. Schmidt, and R. B. Wehrspohn, Adv. Energy Mater. **5**, 1401556 (2015).

31.   F. Bai, W.-K. To, and Z. Huang, J. Phys. Chem. C **117**, 2203 (2013).

32.   R. Ghosh and P. K. Giri, RSC Adv. **6**, 35365 (2016).

33.   Z. Huang, R. Wang, D. Jia, L. Maoying, M. G. Humphrey, and C. Zhang, ACS Appl. Mater. Interfaces **4**, 1553 (2012).

34.   Z. P. Huang, T. Shimizu, S. Senz, Z. Zhang, N. Geyer, and U. Gösele, J. Phys. Chem. C **114**, 10683 (2010).

35.   K.-Q. Peng, A. J. Lu, R. Q. Zhang, and S. T. Lee, Adv. Func. Mater. **18**, 3026 (2008).

36.   Z. P. Huang, T. Shimizu, S. Senz, Z. Zhang, X. X. Zhang, W. Lee, N. Geyer, and U. Gösele, Nano Lett. **9**, 2519 (2009).

37.   B. Jiang, M. Li, Y. Liang, Y. Bai, D. Song, Y. Li, and J. Luo, Nanoscale **8**, 3085 (2016).

38.   X. Jiao, Y. Chao, L. Wu, and A. Yao, J. Mater. Sci.:Mater. Electron **27**, 1881 (2016).

39.   M. Li, Y. Li, W. Liu, L. Yue, R. Li, Y. Luo, M. Trevor, B. Jiang, F. Bai, P. Fu, Y. Zhao, C. Shen, and J. M. Mbengue, Mater. Res. Bull. **76**, 436 (2016).

40.   R. Ouertani, A. Hamdi, C. Amri, M. Khalifa, and H. Ezzaouia, Nanoscale Res. Lett. **9**, 574 (2014).

41.   Y. Wu, Y. Cui, L. Huynh, C. J. Barrelet, D. C. Bell, and C. M. Lieber, Nano Lett. **4**, 433 (2004).